Mapping the spatio-temporal distribution of key vegetation cover properties in lowland river reaches, using digital photography

Authors: Veerle Verschoren[1*], Jonas Schoelynck[1], Kerst Buis[1], Fleur Visser[2], Patrick Meire[1], Stijn Temmerman[1]

1. *University of Antwerp, Department of Biology, Ecosystem Management Research Group, Universiteitsplein 1C, B-2610 Wilrijk, Belgium.*
2. *University of Worcester, Institute of Science and the Environment, Henwick Grove, Worcester WR2 6AJ, UK*

[*]**Corresponding author**

UA - Campus Drie Eiken
Ecosystem Management research group
Universiteitsplein 1
Building C, C1.20
B - 2610 Wilrijk, Belgium

verschoren.veerle@hotmail.com
Tel +32 3 265 22 52
Fax +32 3 265 22 71

Abstract

The presence of vegetation in stream ecosystems is highly dynamic in both space and time. A digital photography technique is developed to map aquatic vegetation cover at species level, which has a very-high spatial and a flexible temporal resolution. A digital single-lens-reflex (DSLR) camera mounted on a handheld telescopic pole is used. The low-altitude (5 m) orthogonal aerial images have a low spectral resolution (Red-Green-Blue), high spatial resolution (~1.9 pixels cm^{-2}, ~1.3 cm length) and flexible temporal resolution (monthly). The method is successfully applied in two lowland rivers to quantify four key properties of vegetated rivers: vegetation cover, patch size distribution, biomass and hydraulic resistance. The main advantages are that the method is: (i) suitable for continuous and discontinuous vegetation covers (ii) of very-high spatial and flexible temporal resolution, (iii) relatively fast compared to conventional ground survey methods, (iv) non-destructive, (v) relatively cheap and easy to use, and (vi) the software is widely available and similar open source alternatives exist. The study area should be less than 10 m wide and the prevailing light conditions and water turbidity levels should be sufficient to look into the water. Further improvements of the images processing are expected in the automatic delineation and classification of the vegetation patches.

Key words: macrophytes, vegetation cover, very high spatial resolution, flexible temporal resolution

Introduction

The presence of aquatic vegetation in river ecosystems tends to be highly variable in space and time. Because of the importance of vegetation in fluvial ecosystems there is a need to efficiently map and monitor this variability. The study described in this paper presents a method for detailed mapping of the dynamic vegetation patterns in rivers.

Macrophytes, or aquatic plants, have different growth forms: exclusively submerged, submerged with floating leaves, exclusively floating or emergent. They occur in single species beds with a continuous cover or in a discontinuous composition of multiple species. The interaction between vegetation and water flow leads to spatial patterns of vegetation patches at reach scale, river sections of 100 to 200 m (Schoelynck et al. 2012). A macrophyte patch can be defined by an area covered by vegetation, which has a finite spatial extent that is larger than an individual shoot but smaller than the entire reach. The size of these vegetation patches varies strongly from a few square decimetre to a few square meter (Gurnell et al. 2006; Sand-Jensen et al. 1999). The size of the individual leaves ranges from several square centimetre to several square decimetre. In temperate mid-latitude climate zones, the development of these vegetation patches has an annual cycle with abundant plant growth in the growth season followed by die-back (Battle and Mihuc 2000; Menendez et al. 2003).

These dynamic growth processes result in frequent changes in key properties of vegetated rivers including vegetation cover, patch size distribution, biomass and hydraulic resistance. These properties in turn affect stream processes, such as: nutrient cycling (Dhote and Dixit 2009; Krause et al. 2011; Seitzinger et al. 2006), the transport of dissolved matter and the retention of particulate matter (Cordova et al. 2008; Horvath 2004; Lamberti et al. 1989), bedload sediment transport (Gibbins et al. 2007) and drift of macro-invertebrates (Extence et al. 1999).

The first of the key properties, macrophyte cover, is an essential parameter used for monitoring of fluvial ecosystems. Macrophytes are for example used as a quality parameter in the assessment of the ecological status of surface water for the Water Framework Directive in Europe (EU 2000). This assessment takes into account the number of species and species abundance. The second key property, the frequency distribution of patch sizes, can be used to investigate spatial self-organisation in river ecosystems. Spatial self-organisation in rivers is the process where large scale patterns develop from disordered initial conditions through small scale feedbacks between plants and the water flow (Lejeune et al. 2004; Rietkerk et al. 2004; Schoelynck et al. 2012). The process is important for ecosystem functioning, since self-organised ecosystems have a higher resilience and resistance to environmental change and a higher productivity compared to homogeneous ecosystems (van de Koppel et al. 2008). Schoelynck et al. (2012) showed the presence of spatial self-organisation of macrophytes patches in lowland rivers. They demonstrated that the size distribution of macrophytes patches can be described by a power-law relationship, which is an indication of self-organisation (Newman 2005; Scanlon et al. 2007). Thirdly, biomass is a crucial parameter in many ecological studies for example for the calculation of mass balances or quantification of nutrient fluxes (Borin and Salvato 2012; Dinka et al. 2004). The parameter values will depend on vegetation extent and species composition. Finally, the hydraulic resistance of a river reach is influenced by obstructions like aquatic vegetation, bed material, the meandering of the river and irregularities in its cross-sections (Chow 1959). Macrophytes increase the hydraulic resistance which leads to reduced stream velocities and increased water levels upstream (De Doncker et al. 2009b). A direct effect of increased water levels is a higher risk of flooding. The effect of macrophytes on the hydraulic resistance is threefold: through vegetation density (e.g. biomass (De Doncker et al. 2009b)), plant characteristics (e.g. growth form (Bal et al. 2011)) and spatial distribution (e.g. cross-sectional blockage (Green 2005b)). In general: high biomass, stiff plants and large cross-sectional blockage all lead to a higher resistance to water flow, which is expressed by a higher Manning roughness coefficient (n) (Chow 1959; Madsen et al. 2001; Vereecken et al. 2006). Recently more detailed hydrodynamic models have been developed, which incorporate such plant features (Verschoren et al. 2016).

To quantify the above-mentioned vegetation parameters and use them for monitoring, modeling and management of river processes, a method is needed that can efficiently map the dynamic patchiness of macrophytes in rivers with a very-high spatial (subcentimetre) and flexible temporal resolution. The detection of fine scale details in structure, texture and pattern on very-high spatial resolution image data allows identification of macrophytes up to species level (Bryson et al. 2013; Visser et al. 2013). Properties like biomass and hydraulic resistance depend strongly on species composition and need flexible temporal resolution (e.g. monthly) data acquisition to catch seasonal variation. Low-altitude image data collection seems the most suitable method to obtain high spatial and flexible temporal resolution data while minimizing the time and cost (Carter et al. 2005; Legleiter 2003).

High resolution low-altitude image data collection techniques proved to be suitable for many ecological studies in intertidal marine environments with a spatial extent between 0.01 - 1 ha and resolutions ranging between 0.5 - 5 cm. Examples are patterns of algae distribution (Guichard 2000), biophysical control of benthic diatom films and macroalgae (van den Wal 2014), the distribution of eelgrass and blue mussel (Barrell and Grant 2015), and terrain models of intertidal rocky shores (Bryson 2013). However, images were mostly obtained at low tides while study sites were not inundated. Due to the absorption of light in water (Visser et al. 2013), limited spatial resolution or high costs (Flynn and Chapra 2014; Husson et al. 2014; Shuchman et al. 2013), it is only relatively recently that more studies started looking at mapping aquatic vegetation in submerged environments, including rivers and lakes (Anker et al. 2014; Silva et al. 2008; Villa et al. 2015). Hyperspectral remote sensing is successfully used to measure the river morphology (Tamminga et al. 2015), to map invasive aquatic vegetation in a delta (Hestir et al. 2008) and submerged macrophytes and green algae in rivers (Anker et al. 2014). However, these hyperspectral images are costly and/or have too low spatial resolution (~1-3 m) to be applied in small streams (stream width <10 m) (Shuchman et al. 2013).

Recent efforts have been undertaken to obtain low-cost, high spatial resolution (subdecimetre to submetre) images, but with a low spectral range. At a resolution of 25 cm, Flynn and Chapra (2014) mapped aquatic submerged vegetation and green algae in small lowland rivers and lakes, and Nezlin et al. (2007) mapped algae and mussels on tidal flats. Higher spatial resolution images were obtained by Husson et al. (2014) (5.6 cm) and Anker et al. (2014) (4 cm) to record aquatic vegetation. However, these resolutions are often still too coarse to distinguish different macrophyte species, which sometimes requires assessment of the shape of individual leaves. A common recommendation from several of the before mentioned studies is the requirement that images should be taken under optimal conditions, e.g. no diffuse light, sun at its highest position, clear water, no ripples. However, this almost never occurs in reality and therefore further limits the applicability of the method and is an additional reason why this technique has not yet become mainstream in river ecosystem research: it is difficult to look into a river trough a camera lens (Visser et al. 2013).

In this paper we present a rapid and cost-effective digital aquatic vegetation cover photography technique based on orthogonal low-altitude images with a very-high (subcentimetre) spatial resolution and flexibility to collect data frequently (monthly or higher) under optimal weather and scene illumination conditions (no diffuse light and the sun at its highest position). We use the collected images to map the spatial distribution of aquatic vegetation at species level in two river ecosystems (± 200 m river reaches) and we demonstrate how the maps are suitable to monitor four key properties of vegetated lowland rivers, namely vegetation cover, patch size distribution, biomass and hydraulic resistance.

Materials and methods

Study area

The data were collected in 2013 in two lowland rivers in the North East of Belgium: Zwarte Nete and Desselse Nete (51° 15’ 3.45” N, 5° 4’ 54.27’’ E) (Fig. 1). Both rivers are characterised by extensive plant growth in summer and are surrounded by pasture, which limits overhanging and other riparian vegetation. The rivers have a low suspended matter concentration (< 50 mg L^{-1}) and the substrate consists of sand (median grain size of 167 µm). The Zwarte Nete has a mean width of 4.4 m, water depth ranges between 0.5 - 0.6 m and discharge between 0.2 - 0.5 m^3 s^{-1}. A reach of 187 m (821 m^2) was mapped where multiple plant species were present. The Desselse Nete is slightly larger with a mean width of 5.4 m, mean water depth of 0.6 - 0.7 m and mean discharge between 0.3 - 0.6 m^3 s^{-1}. Here a reach of 180 m (1123 m^2) was selected, dominated by a single submerged species with floating leaves: *Potamogeton natans* (L.). The following species were present in one or both reaches: submerged species: *Callitriche obtusangula* (Le Gall), *Myriophyllum spicatum* (L.), *Potamogeton pectinatus* (L.) *Ranunculus peltatus* (L.), *Sagittaria* *sagittifolia* (L.), *Sparganium emersum* (L.) and emergent species: *Typha latifolia* (L.) and riparian vegetation (not identified to species level). No exclusively floating species were present.

Image collection

The images were collected with a Nikon D300s DLSR camera with a crop sensor (NikonCorporation, 2009). As inherent to most unmodified cameras, images consisting of three broad spectral bands are obtained (RGB): a blue (400 - 500 nm), a green (500 - 600 nm) and a red band (600 - 700 nm). The files were compressed as JPEG (fine) with an image dimension of 4288 x 2848 pixels and an image size of 12.3 megapixels. The camera was equipped with a Tokina AT-X 116 Pro DX (11-16mm, F2.8) wide angle lens that has a large field-of-view and a distortion of 0.6% (Dxomark). The zoom was set to the widest possible angle and the focus at infinity. The camera was attached with a ball head to a handheld telescopic pole to take low altitude images of the water surface at nadir (Fig. 2a). The lower end of the pole was placed at the river bank. The pole was tilted so that the camera was positioned above the center line of the river at a height of approximately 5 m above the water surface (Fig. 2b). The camera was remotely operated from a laptop (tethered capture), which also provided live view to ensure correct positioning of the image footprint. Both river banks had to be visible in each image. No polarization filter was used as this was not thought to have an effect with the camera at nadir positon. Camera ISO was set to 200 to minimize the noise and a variable aperture to achieve a fast shutter speed (Pekin and Macfarlane 2009). The images generally covered an area of 10 m (along the stream) x 6.5 m (across) (Fig. 3a and 3b).

Multiple images were collected at monthly intervals covering the entire reaches of both rivers from April to September 2013. The distance between two consecutive images was 4 m to ensure sufficient overlap (~30 % overlap). Data was collected on clear days around noon to achieve optimal illumination conditions. The angle between the sun and the camera is approximately 40° between 11 a.m. and 1 p.m. (summertime) in Belgium. Several ground controls points (GCPs) were positioned along the reaches to allow georeferencing of the image mosaics. Both reaches are bounded upstream and downstream by small bridges which were included as GCPs. Geographic coordinates for the GCPs were obtained with a dGPS (Trimble R4 GNSS, Eersel, NL) with an accuracy of 1 cm. The exact coordinates of the river banks were once measured with an electronic theodolite (Total Station, Sokkia set 510k, Capelle a/d Ijssel, NL) with a spatial interval of 2 to 3 m. The coordinates of the river bank were considered as complementary GCPs, which are clearly visible on the images.

Spatio-temporal vegetation cover

Three steps are needed to create vegetation maps at species level: (i) image dehazing and stitching by month and reach, (ii) georeferencing of image mosaics, and (iii) manual delineation of vegetation patches.

Firstly, haze was removed from the images with the Autopano Giga (v. 3.0, Kolor, Francin, FR) software using the Neutralhazer Light Anti-Haze plug-in. The software was then used to create image mosaics along the full river reaches, using image matching algorithms to match up overlapping photographs. For around 10 % of the images the matching process seemed to be affected by reflection, movement of the vegetation with the river current and a homogeneous riparian margin. In these cases we manually added extra control points at matching locations in both images. This hardly affected the time to stitch. The image mosaics were exported as a JPEG. This protocol was repeated for the images of both reaches and for each month. Secondly, in ArcGIS (v. 10.1, ESRI Inc, Redlands, USA) the image mosaics were georeferenced using a spline transformation. It should be noted that the GCPs were not present in all images that formed a mosaic. An example of georeferenced image mosaics is given in Fig 3c and 3d. Thirdly, polygons were drawn manually delineating the vegetation patches. Advantages and limitations of this approach are extensively discussed at the end of this paper. Patches consisted of a single species and had a minimum size of 2 dm^2. For each polygon the type of species was determined from the image (Fig. 3e and 3f). The surface area of each polygon was calculated and summed to obtain the total vegetation cover per reach and per species type.

The manual image classification was validated against independent field measurements of vegetation presence. A conventional grid method (Anker et al. 2014; Champion and Tanner 2000) was used to estimate macrophyte cover on the ground. A rectangular grid of 2.88 by 0.88 m (36 by 11 cells of 0.08 by 0.08 m) was placed at a fixed location monthly in both streams on the same days the images were collected. The presence of macrophytes in each cell is recorded and determined to species level. The image data was resampled to 0.08 m resolution with each cell coded according to the dominant species. The overall accuracy is calculated by comparing the species in each cell of both grids with a true or false evaluation. This is done per month per river. The relative cover for each vegetation class is given for the months with a cover accuracy of less than 95 %.

Patch size distribution

We tested if the frequency distribution of patch sizes can be approached by a power-law relationship. We therefore used the inverse cumulative distribution which is the probability that a patch size (S) is larger than or equal to s (Newman 2005; Scanlon et al. 2007):

$$P\ (S\ \geq s) \sim s^{-\beta} \qquad \text{Eq. 1}$$

with s the size of a patch and β the power-law exponent. A power-law relationship in this context means that the sizes of patches varies strongly with many small patches and relatively few large patches. R (R Core Team 2014) version 3.2.0, was used to fit a standard least squares regression on the log-transformed data.

Biomass

A conversion factor between cover and biomass can be obtained from the literature (e.g. Flynn et al. 2002; Madsen and Adams 1989). However the required input data weren't available for species in our study area, therefore the four dominant species in both rivers (*C. obtusangula, M. spicatum, P.natans, S. emersum*) were sampled monthly to obtain the monthly conversion factor biomass:cover (Tab. 7). Vegetation samples were collected at the date of image acquisition, downstream from the studied reaches to not destruct the natural growth of the vegetation within the study reaches. Each month, three replicates per species were sampled by manually removing the above ground vegetation in a quadrant of 0.5 m x 0.5 m that was placed upon a monotopic vegetation patch. The samples were oven dried (at 70° C for 48 h) and weighed afterwards (dry weight, DW). It has to be noted that in May 2013, no sample could be taken for *C. obtusangula*. Therefore the average was taken of values for April and June to estimate the biomass in that month. The total cover per species per month was obtained through the image analysis. Then the biomass (gDW) per species was calculated monthly by multiplying the species-specific conversion factor biomass:cover (gDW m^{-2}) with the corresponding cover (m^2) . The biomass values were summed for the whole reach and divided by the total surface of the reach to obtain the total biomass (gDW m^{-2}) averaged out over all species and over the whole river reach. Since three replicates were taken, the total biomass consists of three values.

The applied image analysis method aims to quantify vegetation cover in a non-destructive way. However, the validation of the total biomass required mowing of all the vegetation and is therefore a destructive method. We only had the opportunity to use the mowing method in August. On 26 and 28 August 2013 the entire reach in the Desselse Nete and Zwarte Nete was mechanically mowed by cutting most vegetation just above the sediment and removing it from the river. All mowed vegetation from both reaches was immediately weighed (fresh weight, FW). A representative subsample of the biomass consisting of a mixture of all species, was transported to the lab. The subsample was weighed (FW), dried at 70°C for 48h and reweighed (DW). This enabled us to determine a conversion factor between FW and DW for the biomass of the entire reach. R 3.2.0 was used to perform a one-sample t-test to test the difference between the total biomass obtained by the mowing method (one value) and by the image method (mean with standard error based on three values).

Hydraulic resistance

The hydraulic resistance of rivers can be expressed as a Manning coefficient (Chow 1959). The commonly used equation to calculate the Manning coefficient is based on hydraulic parameters and is applicable in vegetated and non-vegetated rivers (Eq. 2, Tab. 1) (Chow 1959). The equation uses the cross-sectional area, discharge, hydraulic radius and the water level slope. The water discharge was measured upstream of both reaches at the same days the images were taken, using an electromagnetic flow meter (Valeport model 801, Totnes, UK) and calculated by the velocity-area method (Bal and Meire 2009). Simultaneously, the water level was measured with two pressure sensors (Eickelkamp, Geisbeek, NL) placed in the water column near the bridges bordering the reach upstream and downstream with a time interval of 20 min. and with an accuracy of 0.5 cm. The elevation difference between the pressure sensors was measured with a RTK-GSP. The water levels are corrected for atmospheric pressure and averaged over 24 h for each sampling campaign. The water level slope in the reaches was calculated by subtracting the upstream and downstream water level, divided by the length of the reach. Additionally, different empirical relationships are used to convert vegetation properties to the Manning coefficient. Based on the data of the surface area coverage of Green (2005a) we found an empirical relationship (Eq. 3, Tab. 1) between the Manning coefficient and the vegetation cover. De Doncker et al. (2009a) fitted an equation (Eq. 4, Tab. 1) based on measurements of the biomass (gDW m^{-2}) and the Manning coefficient. These empirical relationships (Eq. 3 and Eq. 4) are easy to use, but have a limited application potential. They don’t account for the species composition and the horizontal and vertical distribution of the vegetation and are derived for a specific study area. The general Manning coefficient (Eq. 2) is used to validate the empirical equations (Eq. 3 and Eq. 4).

Results

Between 86 and 115 images (~ 1.9 pixels cm^{-2}, ~ 1.3 cm edge length) were taken per reach from which 41 to 56 were selected to construct the image mosaic. The images collection took around one hour per reach per sampling campaign. Reduced illumination of the submerged vegetation target for the April and September data due to low sun angles, made macrophytes less visible in the images. Delineation of the vegetation patches was still possible but the vegetation cover may have been underestimated. Processing of the images took around two days for months with a low vegetation abundance (< 30%) and around three days for months with a high vegetation cover (> 30%).

Spatio-temporal vegetation cover

The total vegetation cover and partial species cover is given per month for the two reaches (Fig. 4). In the Zwarte Nete, the total vegetation cover increases from April to August and suddenly decreases in September due to the scheduled mowing event on 28 August 2013. The dominant species in the Zware Nete are *S. emersum* and *M. spicatum* during the sampling period (Fig. 4a). The natural development of the vegetation cover in the Desselse Nete is different. The growth was disturbed by an extra mowing activity on 25 June 2013 for management and safety regulations. Two months later, a scheduled mowing event took place on 26 August 2013. *P. natans* is the most abundant species in the Desselse Nete each month and recovered completely 8 weeks after the first mowing event (Fig. 4b).

The validation of the image method with the ground survey showed that the accuracy of species identification is very high (>97 %) in the study reach dominated by a single species (Desselse Nete) (Tab. 2). These high values are due the relative simple composition of the vegetation patches, where the whole reach is covered by a single species. On the contrary, the accuracy is less (> 59%) in the river with a heterogeneous composition of multiple species, certainly in months when the vegetation patches are developing (June and July). So the accuracy to determine the exact location of vegetation patches is limited in those months.

For those months with a cover accuracy less than 95 %, the relative cover of each vegetation class is given separately in Tab. 3. The difference in cover between the ground survey method and the image method for each vegetation class is less than 12 %. This means that the cover per vegetation class agrees well between both methods.

Patch size distribution

In total 262 vegetation patches were mapped in August in the Zwarte Nete, of which 143 were *C. obtusangula* patches. The surface area of these patches ranged between 0.04 m^2 and 2.76 m^2. The size frequency distribution of the patches is plotted on a double logarithmic scale (Fig. 5). A significant power-law relationship was found for the upper part of the distribution (least squares regression on the log-transformed data; $p< 0.001$, $R^2 = 0.99$; 59 % of the data).

Biomass

The total biomass per reach is estimated with the image analysis method on a monthly basis (Tab. 4). The monthly conversion factors are given in Tab. 7. The mowed vegetation is immediately weighed (FW) and converted to dry weight with measured the conversion factor FW:DW equal to 10.3. The total biomass (gDW m^{-2}) obtained by the image analysis method does not significantly differ from the biomass (gDW m^{-2}) obtained by the mowing method. The results of the one-sample t-test is a p-value of 0.797 and 0.198 for the Zwarte Nete and Desselse Nete, respectively.

Hydraulic resistance of vegetated rivers

Variation of the Manning coefficient over time is shown for the Zwarte Nete and Desselse Nete in Figure. 6. In the Zwarte Nete the Manning coefficient is based on hydraulic data, Eq. 2, increasing from April to August and decreasing in September to values similar to those of April. The Manning coefficients of the Zwarte Nete calculated with the empirical equations (Eq. 3 and Eq. 4) are well in agreement. The largest difference is found in August with values of 0.26, 0.30 and 0.20 for Eq. 2, Eq. 3 and Eq. 4, respectively. The Manning coefficient based on hydraulic data, Eq. 2, varies between 0.03 and 0.17 in the Desselse Nete. The empirically based Manning coefficients overestimate this value every month up to a factor two. The largest differences are found in the months May, June and August.

Discussion

There is a strong need for new methods to acquire 2D data on the spatial and temporal distribution of vegetation in small rivers. The digital cover photography technique applied in this paper is a useful tool to obtain this detailed 2D information. This method has six main advantages: (i) it can be applied in rivers with any kind of vegetation cover; (ii) it has a very-high spatial resolution, around 1.9 pixels cm^{-2} (~1.3 cm edge length), and a very flexible temporal resolution with the frequency only dependent on availability of suitable weather conditions; (iii) it is relatively fast, two to three days to collect and process the data of a reach of 180 m; (iv) it is non-destructive in contrast to other methods where sampling is involved; (v) the equipment is relatively cheap with a single time cost of approximately € 2000 for the camera, lens, control software and memory card; (vi) the software used to process the data is widely available and similar open source alternatives exist. Tab. 5 shows the performance of the current method in comparison to five other commonly used remote sensing approaches with optical imagery. The spectral range and spectral resolution depends on the sensor for all platforms mentioned in Tab. 5. Manned aircraft imaging can have a wide range of spectral resolution from very narrow band hyperspectral imagery to one very broad band for a panchromatic image. Similarly for satellite imagery, sensors with a high spectral resolution are available. However, these images are of low spectral quality and low spatial resolution. Hyperspectral sensors with a high spectral resolution are available for unmanned aerial vehicles but can only be assembled on larger vehicles and do not achieve the high spatial resolution that can be obtained with RGB cameras. The current method is particularly suitable for studies in river reaches which are difficult to access and require high spatial resolution . In addition, limited technical training is required to pre- and post-process the images. The method can be used in its current stage in relative small study areas for monitoring, modelling and management purposes. Applying this method in larger study areas would require further automatization of image collection, e.g. by attaching the camera to an Unmanned Aerial Vehicle (UAV) (Husson et al. 2014; Tamminga et al. 2015), and image classification, e.g. by applying the OBIA method (Visser et al. 2016).

The image data collection requires suitable light and site conditions. The water needs to be clear (i.e. ideally < 1 m deep and low turbidity) (Visser et al. 2013), and the water velocity should be low to limit stem motion (i.e. ideally < 1 ms^{-1}) (Franklin et al. 2008). These site conditions are similar requirements for the occurrence of macrophytes in the first place (Riis and Biggs 2003). However the water can be temporary less clear after storm events. It this case it is recommended to wait a few days until the concentration of suspended sediment is reduced. Light intensity should be sufficient to penetrate the surface and illuminate the submerged macrophytes. The angle between the sun and the camera should be around 45° to minimize sun glint and maximize the light availability in the water. The time of image collection depends on the latitude of the study area, for example in Belgium (latitude 52 °) this is around noon, between 11 a.m. and 1 p.m., summertime. The image collection can only take place under these specified good weather conditions. This limits the data collection frequency, but for monitoring vegetation very high frequency data is rarely needed. Techniques currently under development may in the near future allow the removal of remaining surface reflection (Hardesty 2015). Other requirements are related to the study area itself. The rivers and streams should be relative small, i.e. <10 m wide, which is the equivalent of the spatial extent covered by one image, and at least one river bank should be accessible and stable enough to position the pole. Yet these limitations to the study area can be overcome by attaching the camera to an Unmanned Aerial Vehicle (UAV) (Husson et al. 2014; Tamminga et al. 2015), or to a helium balloon, or by attaching the pole to the bow of a boat (Lirman and Deangelo 2007). This makes it possible to collect similar resolution data from close to the water surface of larger rivers. However, helium balloons need to be sufficiently big to carry a DSLR camera, which makes them rather impractical and in the long-run quite expensive platforms (due to the cost of helium). UAVs are a good alternative since battery life is improving year on year. Currently the only disadvantages of a rotary-winged UAV platform are (i) the need for training to actually fly the vehicle, which may involve some costly training; (ii) the purchase and insurance of suitable quality UAV and camera; (iii) the transport of larger UAVs. UAVs are therefore the platform of choice for further development of the method proposed in this paper.

The image processing as it was done is this study works well, yet improvements are possible to delineate and identify the vegetation patches. This study used a manual interpretation based on expert judgement, which is a sound method to separate between different species (Husson et al.2014), because the manual delineation and identification uses many image elements like size, shape, shadow, colour, texture, pattern, location and surroundings (Colwell 1960; Tempfli et al. 2009). However, the observer bias can still be present since this method makes use of manual decision rules concerning the exact edge of the vegetation patches. In the study reach dominated by a single species the accuracy is very high (>97 %). These high values are due to the relative simple composition of the vegetation patches, where the whole reach is covered by a single species (Desselse Nete). On the contrary, the accuracy is less (> 59%) in the river with a heterogeneous composition of multiple species (Zwarte Nete), certainly in months when the vegetation patches are developing (June and July). If we compare the relative cover of each vegetation class between the image method and ground survey, differences are less than 12 %. The images method proved to be suitable to estimate the relative cover of each vegetation class in rivers with a continuous and discontinuous vegetation cover. However, it is difficult to map the exact location of all vegetation patches in rivers with heterogeneous vegetation cover. This is due to the movement of the vegetation patches by the flowing water and the relatively simple image processing.

Another limitation is the detection of rare species which are normally not abundantl, e.g. *C. obtusangula* was detected by the ground survey in June and July in the Zwarte Nete but not by the image method. The last limitation is the separation of multi-layered plant communities, e.g. *P. natans* was classified as *S. emersum* in August (Desselse Nete), while only a few leaves of *S. emersum* where present on top of *P. natans*. Similar limitations are found by Anker et al. (2014). From the images, plant growth form (submerged, submerged with floating leaves, emergent) can be easily recognized, as well as the species identification up to genus level. A classification up to species level is possible, but requires knowledge of the species present in the reach. This information can simply be obtained during the collection of the images at the field site. Automatic classification methods based on variation in spectral signatures of different vegetation types could not be used to automatically delineate and identify vegetation patches under these specific circumstances. The varying incidences of light, the prevailing sub-optimal light conditions during the sampling campaign and submergence depth of the vegetation all caused complications for automated species detection (Visser et al. 2013). We acknowledge this drawback on the manual image processing, which increases the cost of data processing and may make this method no longer as cost-effective. Attention should be given to reduce phenological (space and time) differences in the classification to make this technique suitable for long term monitoring. Two solutions have been proposed: (i) convert the Red-Green-Blue colors to the green chromatic coordinate ($G/[R + G + B]$), (ii) use the 90th percentile of all daytime values within a three-day window around the centre day (Dronova 2017; Sonnentag et al. 2012). However, it may be not straightforward to apply similar algorithms to submerged aquatic vegetation where relative variation in Red-Green-Blue values at any point can differ due to water depth differences. Alternative image analysis approaches such as object based image analysis (OBIA) are less reliant on spectral information and may mitigate for such conditions, however applications of such approaches in submerged environments are still in a developmental stage (Visser et al. 2016). OBIA is currently applied in other ecosystems. For example Laba et al. (2010) used a maximum-likelihood classification in tidal marshes, which resulted in a classification accuracy between 45 and 77 %. In offshore submerged environments OBIA based approaches have so far achieved good results for mapping coarse vegetation and substrate classes. For example, the extent of seagrass habitat was mapped by Baumstark et al. (2016), showing in a slightly higher accuracy using OBIA (78%) compared to photo-interpretation (71%).

The image analysis method proved suitable for measuring the spatio-temporal vegetation cover, which is a primary parameter for monitoring vegetated ecosystems. For instance within the Water Framework Directive, it is essential for long-term monitoring of vegetation abundance (Hering et al. 2010). Changes in abundance and location of the vegetation were derived directly from the image data. For example the regrowth capacity of *P. natans* was high after the mowing event in June, and pre-mowed cover values were reached within 8 weeks, which is similar to other macrophyte species (Bal et al. 2006). Other, more conventional methods to estimate vegetation cover data range from fast methods with a high observer bias due to expert judgement (Tansley scaling method based on 5 classes) to more detailed scaling methods, which have a higher accuracy, but are more time consuming and require substantial expert knowledge (Braun-Blanquet scaling method based on 9 classes (Blanquet 1928)) and Londo scaling method based on at least 21 classes (Londo 1976)). These methods have two main disadvantages. Firstly, abundance class errors are difficult to correct even with substantial expert knowledge (Wiederkehr et al. 2015). Secondly, the classification of the cover makes use of discontinuous class scales, which are less accurate and can hamper data analyses. Hence the image analysis method fulfils the requirement of a more objective quantification of the cover with a continuous cover scale with high spatial and flexible temporal resolution.

The cover maps were also used in this study to investigate the presence of spatial self-organisation of macrophytes in lowland rivers. A significant power-law relationship of the frequency distribution of the patch sizes is found, which is an indication of spatial self-organisation (Newman 2005; Scanlon et al. 2007). This is in agreement with a study of Schoelynck et al. (2012), who investigated the spatial self-organisation of macrophytes in the same reach in the Zwarte Nete in 2008. In the study of Schoelynck et al. (2012) the exact location of all vegetation patches was determined using an electronic theodolite. It took roughly three weeks to map the whole reach, which is much slower in comparison with the new method, were we needed 1 hour to collect the images and two to three days to process the data. So obtaining spatial information of vegetation is much faster compared to conventional methods.

From the cover data, biomass can be derived using simple non-destructive cover:biomass conversion factors. These conversion factors can be determined for the specific field site or can be obtained from literature (e.g. Madsen and Adams (1989); Flynn et al. (2002)). The biomass (gDW m^{-2}) estimated by the image analysis method was compared to the biomass obtained from the scheduled mowing method. The biomass obtained by the two methods does not significantly differ for either of the two reaches. The relatively small differences may be attributed to inaccuracies in both methods. During the scheduled mowing, the biomass could have been slightly overestimated when non-plant materials like sediment, stones and dead wood were removed too, which may have added up to the total fresh weight, or underestimated the latter when not all the vegetation was removed. However, we only assessed the biomass in a month with high biomass. Higher relative difference in biomass might be expected when less biomass is present, but this would result in low absolute differences. The image analysis method may also have certain flaws and uncertainties involving the estimation of the species-specific biomass obtained by the plots. The within species variation of the biomass may not be fully captured by three replicas (e.g. by depth variance of the river and of the vegetation). The image analysis method doesn't account for variability in the density. Classic methods of biomass estimation are based on destructive measures of the biomass (mowing, harvesting), which disturb the follow-up of natural vegetation development during the growth season (Wood et al. 2012).

The difference between the Manning coefficient based on empirical relationships and the one based on hydraulic data differs less than 23 % in the Zwarte Nete and less than 37% in the Desselse Nete. The empirical relationships don't account for the species composition and horizontal and vertical distribution of the vegetation, which are different in both rivers and are major determining factors of the hydraulic resistance of the reach. The Zwarte Nete is dominated by submerged vegetation and this vegetation type has similar effects on the hydraulic resistance as the vegetation used to construct Eq. 2 and Eq. 3. The Desselse Nete is dominated by the floating species *P. natans,* which is a more open species that concentrates the majority of the biomass near the water surface, which leads to a limited interaction with the water flow: rivers with macrophytes can have a 2 to 7-fold increase of the resistance for floating (Green 2005a) and submerged (Bal and Meire 2009) species, respectively, compared to rivers without vegetation. The same vegetation biomass or cover will therefore result in a lower hydraulic resistance. Detailed 2D hydrodynamic models can be used to quantify more accurately the hydraulic resistance created by the vegetation based on plant density, species characteristics and spatial distribution of the vegetation (Verschoren et al. 2015). Accurate 2D spatio-temporal vegetation cover data, as obtained by the digital cover photography technique, is indispensable to calibrate and validate these models. The spatial distribution of the vegetation is a direct input to these models. Therefore these models account for the exact location of all vegetation patches and the different plant characteristics of all species. This is a major leap forward for engineers and water managers in the fine tuning of the hydrodynamic models of vegetated rivers.

Conclusions

We successfully applied a digital cover photography technique based on orthogonal aerial images with a very-high spatial (subcentimetre) and flexible temporal (monthly) resolution. The produced vegetation maps were used to assess four key properties of vegetated lowland rivers which are important for monitoring, modelling and management, being spatio-temporal variation in vegetation cover, patch size distribution, biomass and hydraulic resistance.

The main limitations are related to the study area itself, which should be limited in size, and the prevailing light conditions should be sufficient to look into the water. Improvements in the images processing are situated in the automatic delineation and classification of the vegetation patches.

Acknowledgements

The funding for this research was partly provided by the Research Fund Flanders (FWO-, project no. G.0290.10) via the multidisciplinary research project 'Linking optical imaging techniques and 2D-modelling for studying spatial heterogeneity in vegetated streams and rivers' (University of Antwerp and University of Ghent) and party by Province of Antwerp, departement Leefmilieu, dienst Integraal Waterbeleid (Report number ECOBE – 014 – R179). V.V. thanks the Institute for the Promotion of Innovation through Science and Technology in Flanders (IWT-Vlaanderen) for personal research funding. J.S. is a postdoctoral fellow of FWO (project no. 12H8616N).

References

Anker, Y., Y. Hershkovitz, E. Ben Dor & A. Gasith, 2014. Application of Aerial Digital Photography for Macrophyte Cover and Composition Survey in Small Rural Streams. River Res Appl 30(7):925-937.

Apollo Mapping, 2016. RapidEye. In. https://apollomapping.com/imagery/medium-resolution-satellite-imagery.

Bal, K. D. & P. Meire, 2009. The Influence of Macrophyte Cutting on the Hydraulic Resistance of Lowland Rivers. J Aquat Plant Manage 47:65-68.

Bal, K. D., E. Struyf, H. Vereecken, P. Viaene, L. De Doncker, E. de Deckere, F. Mostaert & P. Meire, 2011. How do macrophyte distribution patterns affect hydraulic resistances? Ecol Eng 37(3):529-533.

Bal, K. D., S. Van Belleghem, E. De Deckere & P. Meire, 2006. The re-growth capacity of sago pondweed following mechanical cutting. J Aquat Plant Manage 44:139-141.

Barrell, J. & J. Grant, 2015. High-resolution, low-altitude aerial photography in physical geography: A case study characterizing eelgrass (Zostera marina L.) and blue mussel (Mytilus edulis L.) landscape mosaic structure. Prog Phys Geog 39(4):440-459.

Battle, J. M. & T. B. Mihuc, 2000. Decomposition dynamics of aquatic macrophytes in the lower Atchafalaya, a large floodplain river. Hydrobiologia 418:123-136. Blanquet, B., 1928. Pflanzensoziologie. Grundzüge der Vegegtationskunde, Berlin 1.ed. Berlin.

Baumstark R., R. Duffey & R. Pu, 2016. Mapping seagrass and colonized hard bottom in Springs Coast, Florida using WorldView-2 satellite imagery. Estuarine, Coastal and Shelf Science 181:83-92.Borin, M. & M. Salvato, 2012. Effects of five macrophytes on nitrogen remediation and mass balance in wetland mesocosms. Ecol Eng 46:34-42.

Bryson, M., M. Johnson-Roberson, R. J. Murphy & D. Bongiorno, 2013. Kite Aerial Photography for Low-Cost, Ultra-high Spatial Resolution Multi-Spectral Mapping of Intertidal Landscapes. Plos One 8(9).

Carter, G. A., A. K. Knapp, J. E. Anderson, G. A. Hoch & M. D. Smith, 2005. Indicators of plant species richness in AVIRIS spectra of a mesic grassland. Remote Sens Environ 98(2-3):304-316.

Champion, P. D. & C. C. Tanner, 2000. Seasonality of macrophytes and interaction with flow in a New Zealand lowland stream. Hydrobiologia 441(1-3):1-12.

Chow, V. T., 1959. Open-channel hydraulics. McGraw-Hill, New York, USA.

Colwell, R., 1960. Manual of photographic interpretation Washington, DC.

Cordova, J. M., E. J. Rosi-Marshall, J. L. Tank & G. A. Lamberti, 2008. Coarse particulate organic matter transport in low-gradient streams of the Upper Peninsula of Michigan. J N Am Benthol Soc 27(3):760-771.

De Doncker, L., P. Troch, R. Verhoeven, K. Bal, N. Desmet & P. Meire, 2009a. Relation between Resistance Characteristics Due to Aquatic Weed Growth and the Hydraulic Capacity of the River Aa. River Res Appl 25(10):1287-1303.

De Doncker, L., P. Troch, R. Verhoeven, K. Bal, P. Meire & J. Quintelier, 2009b. Determination of the Manning roughness coefficient influenced by vegetation in the river Aa and Biebrza river. Environ Fluid Mech 9(5):549-567.

Dhote, S. & S. Dixit, 2009. Water quality improvement through macrophytes-a review. Environ Monit Assess 152(1-4):149-153.

Dinka, M., E. Agoston-Szabo & I. Toth, 2004. Changes in nutrient and fibre content of decomposing Phragmites australis litter. Int Rev Hydrobiol 89(5-6):519-535.

Dronova, I. 2017. Environmental heterogeneity as a bridge between ecosystem service and visual quality objectives in management, planning and design. Landscape and Urban Planning 163:90-106.

EU, 2000. 2000/60/EC. A framework for the Community action in the field of water policy, or short: The EU Water Framework Directive Directive 2000/60/EC, The European Parliament and the European Council of Ministers. Brussels, Belgium.

Extence, C. A., D. M. Balbi & R. P. Chadd, 1999. River flow indexing using British benthic macroinvertebrates: A framework for setting hydroecological objectives. Regul River 15(6):543-574.

Flynn, K. F. & S. C. Chapra, 2014. Remote Sensing of Submerged Aquatic Vegetation in a Shallow Non-Turbid River Using an Unmanned Aerial Vehicle. Remote Sens-Basel 6(12):12815-12836.

Flynn, N. J., D. L. Snook, A. J. Wade & H. P. Jarvie, 2002. Macrophyte and periphyton dynamics in a UK Cretaceous chalk stream: the River Kennet, a tributary of the Thames. Sci Total Environ 282:143-157.

Foody, G. M., 2002. Status of land cover classification accuracy assessment. Remote Sens Environ 80(1):185-201.

Franklin, P., M., Dunbar & P. Whitehead, 2008. Flow controls on lowland river macrophytes: A review. Sci Total Environ 400(1-3):369-378.

Gibbins, C., D. Vericat & R. J. Batalla, 2007. When is stream invertebrate drift catastrophic? The role of hydraulics and sediment transport in initiating drift during flood events. Freshwater Biol 52(12):2369-2384.

Green, J. C., 2005a. Comparison of blockage factors in modelling the resistance of channels containing submerged macrophytes. River Res Appl 21(6):671-686.

Green, J. C., 2005b. Modelling flow resistance in vegetated streams: review and development of new theory. Hydrol Process 19(6):1245-1259.

Guichard, F., E. Bourget & J. P. Agnard, 2000. High-resolution remote sensing of intertidal ecosystems: A low-cost technique to link scale-dependent patterns and processes. Limnol Oceanogr 45(2):328-338.

Gurnell, A. M., M. P. van Oosterhout, B. de Vlieger & J. M. Goodson, 2006. Reach-scale interactions between aquatic plants and physical habitat: River Frome, Dorset. River Res Appl 22(6):667-680.

Hardesty, L., 2015. Removing reflections from photos taken through windows: new algorithm exploits multiple reflections in individual images to distinguish reflection from transmission. In: Massachusetts Institute of Technology.

Hering, D., A. Borja, J. Carstensen, L. Carvalho, M. Elliott, C. K. Feld, A. S. Heiskanen, R. K. Johnson, J. Moe, D. Pont, A. L. Solheim & W. Van De Bund, 2010. The European Water Framework Directive at the age of 10: A critical review of the achievements with recommendations for the future. Sci Total Environ 408(19):4007-4019.

Hestir, E. L., S. Khanna, M. E. Andrew, M. J. Santos, J. H. Viers, J. A. Greenberg, S. S. Rajapakse & S. L. Ustin, 2008. Identification of invasive vegetation using hyperspectral remote sensing in the California Delta ecosystem. Remote Sens Environ 112(11):4034-4047.

Horvath, T. G., 2004. Retention of particulate matter by macrophytes in a first-order stream. Aquat Bot 78(1):27-36.

Husson, E., O. Hagner & F. Ecke, 2014. Unmanned aircraft systems help to map aquatic vegetation. Appl Veg Sci 17(3):567-577.

Krause, S., D. M. Hannah, J. H. Fleckenstein, C. M. Heppell, D. Kaeser, R. Pickup, G. Pinay, A. L. Robertson & P. J. Wood, 2011. Inter-disciplinary perspectives on processes in the hyporheic zone. Ecohydrology 4(4):481-499.

Lamberti, G. A., S. V. Gregory, L. R. Ashkenas, R. C. Wildman & A. D. Steinman, 1989. Influence of Channel Geomorphology on Retention of Dissolved and Particulate Matter in a Cascade Mountain Stream. Us for Serv T R Psw 110:33-39.

Laba, M., B. Blair, R. Downs, B. Monger, W. Philpot, S. Smith, P. Sullivan & P. C. Baveye, 2010. Use of textural measurements to map invasive wetland plants in the Hudson River National Estuarine Research Reserve with IKONOS satellite imagery. Remote Sensing of Environment 114:876-886.

Legleiter, C. J., 2003. Spectrally driven classification of high spatial resolution, hyperspectral imagery: A tool for mapping in-stream habitat. Environ Manage 32(3):399-411.

Lejeune, O., M. Tlidi & R. Lefever, 2004. Vegetation spots and stripes: Dissipative structures in arid landscapes. Int J Quantum Chem 98(2):261-271.

Lirman, D. & G. Deangelo, 2007. Geospatial video monitoring of benthic habitats using the Shallow-Water Positioning System (SWaPS). Oceans-Ieee:1176-1180.

Londo, G., 1976. The decimal scale for releves of permanent quadrats, vol 33.

Madsen, J. D. & M. S. Adams, 1989. The Distribution of Submerged Aquatic Macrophyte Biomass in a Eutrophic Stream, Badfish Creek - the Effect of Environment. Hydrobiologia 171(2):111-119.

Madsen, J. D., P. A. Chambers, W. F. James, E. W. Koch & D. F. Westlake, 2001. The interaction between water movement, sediment dynamics and submersed macrophytes. Hydrobiologia 444(1-3):71-84.

Masek, J. G., D. J. Hayes, M. J. Hughes, S. P. Healey & D. P. Turner, 2015. The role of remote sensing in process-scaling studies of managed forest ecosystems. Forest Ecol Manag 355:109-123.

Menendez, M., O. Hernandez & F. A. Comin, 2003. Seasonal comparisons of leaf processing rates in two Mediterranean rivers with different nutrient availability. Hydrobiologia 495(1-3):159-169.

Mitchell, J. J., R. Shrestha, L. P. Spaete & N. F. Glenn, 2015. Combining airborne hyperspectral and LiDAR data across local sites for upscaling shrubland structural information: Lessons for HyspIRI. Remote Sens Environ 167:98-110.

NASA, 2016. MODIS, Moderate Resolution Imaging Spectroradiometer. In. http://modis.gsfc.nasa.gov.

Newman, M. E. J., 2005. Power laws, Pareto distributions and Zipf's law. Contemporary Physics 46(5):323-351.

Nezlin, N. P., K. Kamer & E. D. Stein, 2007. Application of color infrared aerial photography to assess macroalgal distribution in an eutrophic estuary, upper Newport Bay, California. Estuar Coast 30(5):855-868.

Pekin, B. & C. Macfarlane, 2009. Measurement of Crown Cover and Leaf Area Index Using Digital Cover Photography and Its Application to Remote Sensing. Remote Sens-Basel 1(4):1298-1320.

R Core Team, 2014. R: A language and environment for statistical computing.

Rango, A., A. Laliberte, K. Havstad, C. Winters, C. Steele & D. Browning, 2010. Rangeland Resource Assessment, Monitoring, and Management Using Unmanned Aerial Vehicle-Based Remote Sensing. Int Geosci Remote Se:608-611.

Rietkerk, M., S. C. Dekker, P. C. de Ruiter & J. van de Koppel, 2004. Self-organized patchiness and catastrophic shifts in ecosystems. Science 305(5692):1926-1929.

Riis, T. & B. J. F. Biggs, 2003. Hydrologic and hydraulic control of macrophyte establishment and performance in streams. Limnol Oceanogr 48(4):1488-1497.

Sand-Jensen, K., K. Andersen & T. Andersen, 1999. Dynamic properties of recruitment, expansion and mortality of macrophyte patches in streams. Int Rev Hydrobiol 84(5):497-508.

Satellite Imaging Corporation, 2016. Ikonos Satellite Sensor. In. http://www.satimagingcorp.com/satellite-sensors/ikonos/.

Scanlon, T. M., K. K. Caylor, S. A. Levin & I. Rodriguez-Iturbe, 2007. Positive feedbacks promote power-law clustering of Kalahari vegetation. Nature 449(7159):209-U4.

Schoelynck, J., T. De Groote, K. Bal, W. Vandenbruwaene, P. Meire & S. Temmerman, 2012. Self-organised patchiness and scale-dependent bio-geomorphic feedbacks in aquatic river vegetation. Ecography 35(8):760-768.

Seitzinger, S., J. A. Harrison, J. K. Bohlke, A. F. Bouwman, R. Lowrance, B. Peterson, C. Tobias & G. Van Drecht, 2006. Denitrification across landscapes and waterscapes: A synthesis. Ecol Appl 16(6):2064-2090.

Shuchman, R. A., M. J. Sayers & C. N. Brooks, 2013. Mapping and monitoring the extent of submerged aquatic vegetation in the Laurentian Great Lakes with multi-scale satellite remote sensing. J Great Lakes Res 39:78-89.

Silva, T. S. F., M. P. F. Costa, J. M. Melack & E. M. L. M. Novo, 2008. Remote sensing of aquatic vegetation: theory and applications. Environ Monit Assess 140(1-3):131-145.

Sonnentag, O., Hufkens, K., Teshera-Sterne, C., Young, A.M., Friedl, M.A., Braswell, B.H., Miliman, T., O'Keefe, J., Richardson, A.D. (2012), Digital repeat photography for phenological research in forest ecosystems. Agricultural and Forest Meteorology, 152, 159-177.

Tamminga, A., C. Hugenholtz, B. Eaton & M. Lapointe, 2015. Hyperspatial Remote Sensing of Channel Reach Morphology and Hydraulic Fish Habitat Using an Unmanned Aerial Vehicle (Uav): A First Assessment in the Context of River Research and Management. River Res Appl 31(3):379-391.

Tempfli, K., N. Kerle, G. Huurneman & L. Janssen, 2009. Principles of remote sensing, Enschede, NL.

U.S. Department of the Interior & U.S. Geological Survey, 2016. Landsat Missions. In. http://landsat.usgs.gov.

van de Koppel, J., J. C. Gascoigne, G. Theraulaz, M. Rietkerk, W. M. Mooij & P. M. J. Herman, 2008. Experimental Evidence for Spatial Self-Organization and Its Emergent Effects in Mussel Bed Ecosystems. Science 322(5902):739-742.

van der Wal, D., J. van Dalen, A. Wielemaker-van den Dool, J. T. Dijkstra & T. Ysebaert, 2014. Biophisical contral of the intertidal benthic macroalgae revealed by high-frequency multispectral camera images. J Sea Res 90:111-120.

Vereecken, H., J. Baetens, P. Viaene, F. Mostaert & P. Meire, 2006. Ecological management of aquatic plants: effects in lowland streams. Hydrobiologia 570:205-210.

Verschoren, V., D. Meire, J. Schoelynck, K. Buis, K. D. Bal, P. Troch, P. Meire & S. Temmerman, 2016. Resistance and reconfiguration of natural flexible submerged vegetation in hydrodynamic river modelling Environ Fluid Mech 16(1), 245-265.

Villa, P., M. Bresciani, R. Bolpagni, M. Pinardi & C. Giardino, 2015. A rule-based approach for mapping macrophyte communities using multi-temporal aquatic vegetation indices. Remote Sens Environ 171:218-233.

Visser, F., C. Wallis & A. M. Sinnott, 2013. Optical remote sensing of submerged aquatic vegetation: Opportunities for shallow clearwater streams. Limnologica 43(5):388-398.

Visser, F., K. Buis, V. Verschoren & J. Schoelynck, 2016. Mapping of submerged aquatic in rivers from very high-resolution image data, using object-based image analysis combined with expert knowledge. Hydrobiologia:19 doi:10.1007/s10750-016-2928-y.

Wiederkehr, J., C. Grac, M. Fabregue, B. Fontan, F. Labat, F. Le Ber & M. Tremolieres, 2015. Experimental study of uncertainties on the macrophyte index (IBMR) based on species identification and cover. Ecol Indic 50:242-250.

Wood, K. A., R. A. Stillman, R. T. Clarke, F. Daunt & M. T. O'Hare, 2012. Measuring submerged macrophyte standing crop in shallow rivers: A test of methodology. Aquat Bot 102:28-33.

Tables

Table 1: Overview of the equations used to calculate the Manning coefficient, n (s $m^{-1/3}$). Eq. 2 is used to calculate the Manning coefficient, with A (m^2) cross-sectional area, Q (m^3 s^{-1}) discharge, R (m) hydraulic radius, S (m m^{-1}) water level slope, for which all parameters are measured in both reaches of the study area. Eq. 3 and Eq. 4 are empirical relationships between the Manning coefficient and the vegetation cover (%) and Manning coefficient and the biomass (g DW m^{-2}), respectively All parameters are derived from the digital maps.

Reference	**Equation**	**Number**
Chow et al. (1956)	$n = \frac{A}{Q} * R^{2/3} * S^{1/2}$	Eq. 2
Green (2005)	$n = 0.0438 \exp(0.0200 * cover)$	Eq. 3
De Doncker et al. (2009)	$n = 0.4628 - 0.3998 \exp(-0.0047 * biomass)$	Eq. 4

Table 2: The accuracy (%) of the species identification of the image method compared to the ground survey method per month per river. The accuracy is based on species level; for each grid cell (n=396) the species is compared between the image method and the ground survey method.

Month	**April**	**May**	**June**	**July**	**August**	**September**
Zwarte Nete	100	100	66.4	59.6	84.8	93.7
Desselse Nete	100	100	100	100	97.0	100

Table 3: Percentage vegetation cover (%) estimated by the image method and the ground survey method (GS) for June, July, August and September in the Zwarte Nete.

Month	**June**		**July**		**August**		**September**	
Method	GS	Image	GS	Image	GS	Image	GS	Image
C. obtusangula	2.3	0.0	2.0	0.0	2.5	2.5	0.0	0.0
M. spicatum	-	-	-	-	-	-	-	-
P. pectinatus	1.3	0.0	25.5	24.0	5.1	0.0	-	-
S. emersum	32.3	29.6	62.1	59.3	86.4	97.5	4.6	6.1
Riparian vegetation	-	-	-	-	-	-	-	-
Bare sediment	64.1	70.4	10.4	16.6	1.0	0.0	95.5	94.0

Table 4: Total biomass (gDW m^{-2}) per month in both rivers. The biomass is estimated by the image analysis method and by mowing method when all vegetation was removed and weighed.

Month	April	May	June	July	August	September
Zwarte Nete						
Image	0	3.3 ± 0.1	11.4 ± 3.0	56.8 ± 5.9	187.5 ± 34.2	10.8 ± 1.3
Mowing	-	-	-	-	193.3	-
Desselse Nete						
Image	0.9	65.8 ± 8.8	101.6 ± 26.4	36.7 ± 7.9	150.4 ± 24.4	13.8 ± 3.5
Mowing	-	-	-	-	123.6	-

Table 5: Comparison of the current method with fiveother remote sensing approaches using optical imagery and ground level visual survey. The features where the current method performs good are highlighted in bold.

	Spatial resolution (pixel edge length)	Temporal resolution	Spectral region	Operation cost	Collection cost	Spatial extent	Weather dependency	Knowledge requirements (obtaining, processing)
This study	**< 1 cm**	**Flexible**	RGB	Low (man hours, consumables)	**Low**	m^2	**Low (sun)**	**Low**
Kite, blimp and balloon photography (Barrell and Grant 2015; Bryson et al. 2013; Guichard et al. 2000)	< 5 cm	Flexible	RBG NIR	Low (man hours, consumables)	Medium	m^2	Medium (sun, wind speed)	Medium
Unmanned aerial vehicles (Rango et al. 2010)	1-10 cm (dependent on sensor and flight height)	Flexible	RBG NIR	High (training, man hours, post-processing)	Medium	m^2 - hm^2	Medium (sun, wind speed)	High
Manned aircraft imaging	0.3 - 5m (dependent on flying height)	Flexible	RGB NIR MIR	High (plane charter, post-processing)	High	m^2 - km^2	High (sun, sky conditions)	High
Freely available satellite images (NASA 2016; U.S. Department of the Interior and U.S. Geological Survey 2016)	> 5 m	Fixed Several/year (dependent on location and resolution)	RGB NIR MIR	0	0	> 1 km^2	High (sun, sky conditions)	Medium
Commercial satellite images (Apollo Mapping 2016; Satellite Imaging Corporation 2016)	0.5-5 m	Fixed 14-100 days (dependent on location and resolution)	RGB NIR MIR	0	High	> 1 km^2	High (sun, sky conditions)	Medium
Ground level visual survey	Variable	Flexible	-	High	-	m^2	None	Low

Figures

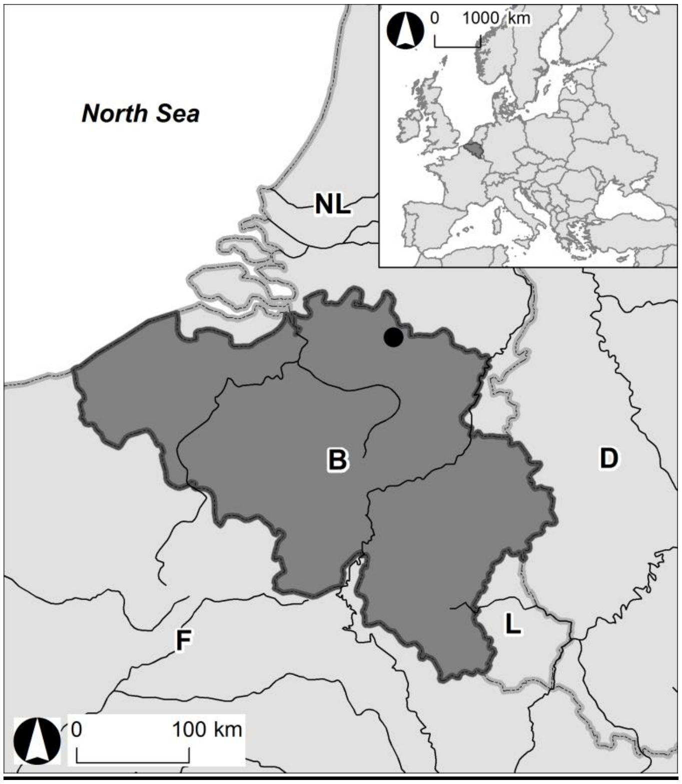

Figure 1: The location of the study area is indicated with a black dot in the North East of Belgium. Insert: the location of Belgium in Europa is shown in dark grey.

Figure 2: Illustrations of the image collection in the field. **(a)** The DSLR camera is attached with a ball head to a handheld telescopic pole to take orthogonal images. **(b)** One person holds the pole with camera tilted in order to position the camera at a height of 5 m above the water surface. A second person checks with a live view on a laptop that both river banks are visible on each image and takes the images with tethered capture**.**

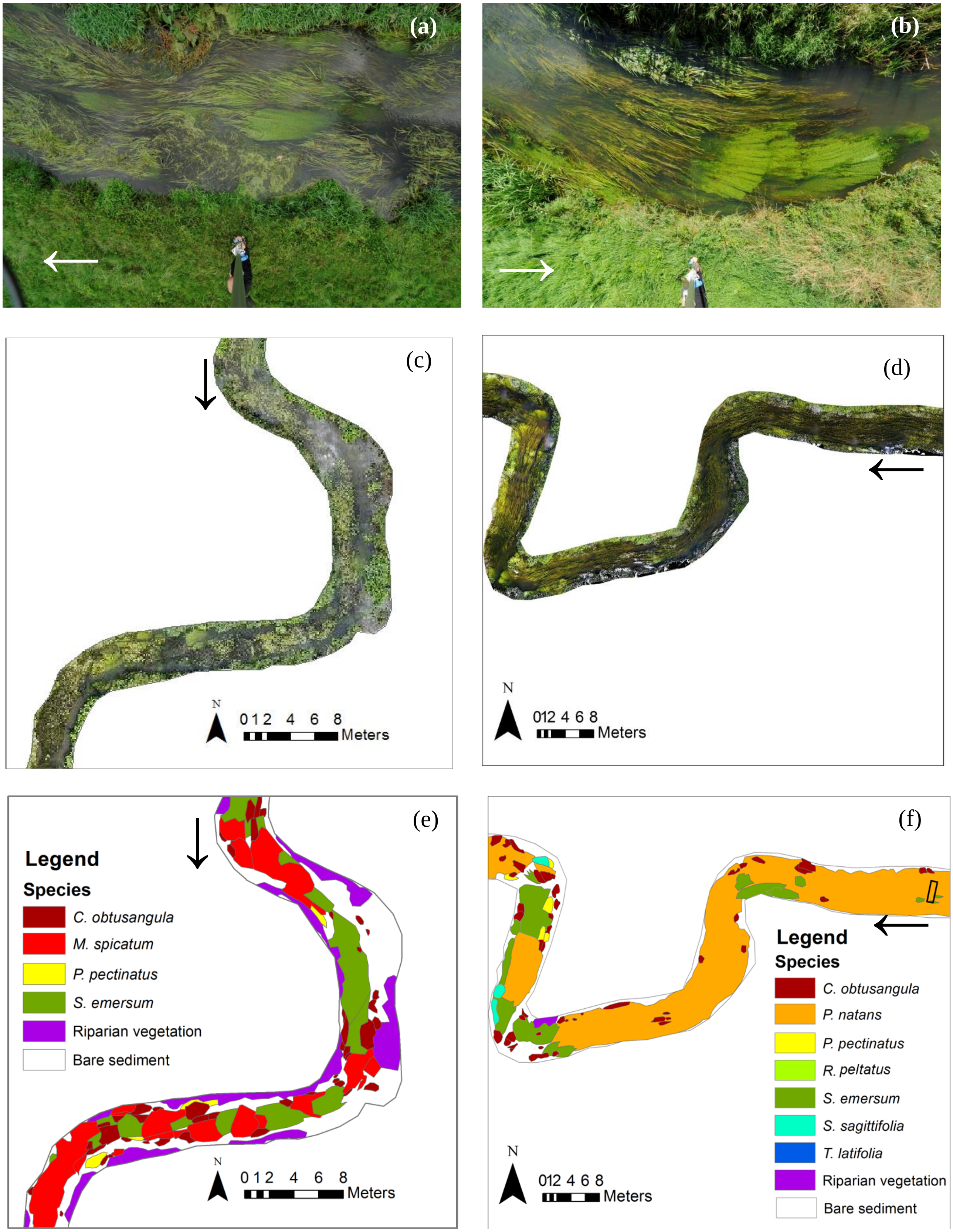
(a)
(b)
(c)
N
0 1 2 4 6 8
Meters
(d)
N
012 4 6 8
Meters
(e)
Legend
Species
C. obtusangula
M. spicatum
P. pectinatus
S. emersum
Riparian vegetation
Bare sediment
N
0 1 2 4 6 8
Meters
(f)
Legend
Species
C. obtusangula
P. natans
P. pectinatus
R. peltatus
S. emersum
S. sagittifolia
T. latifolia
Riparian vegetation
Bare sediment
N
012 4 6 8
Meters

Figure 3: Examples are given of the image collection, processing and analysis in the **(a, c, e)** Zwarte Nete and the **(b, d, e)** Desselse Nete on the 13th of August 2013. Illustrations are shown of (a, b) individual images taken with a DSLR camera attached to a pole, (c, d) a plan view of a part of the image mosaic, (e, f) vegetation map with colors indicating the species and the location of the ground survey (black rectangular). The water flow direction is indicated with an arrow.

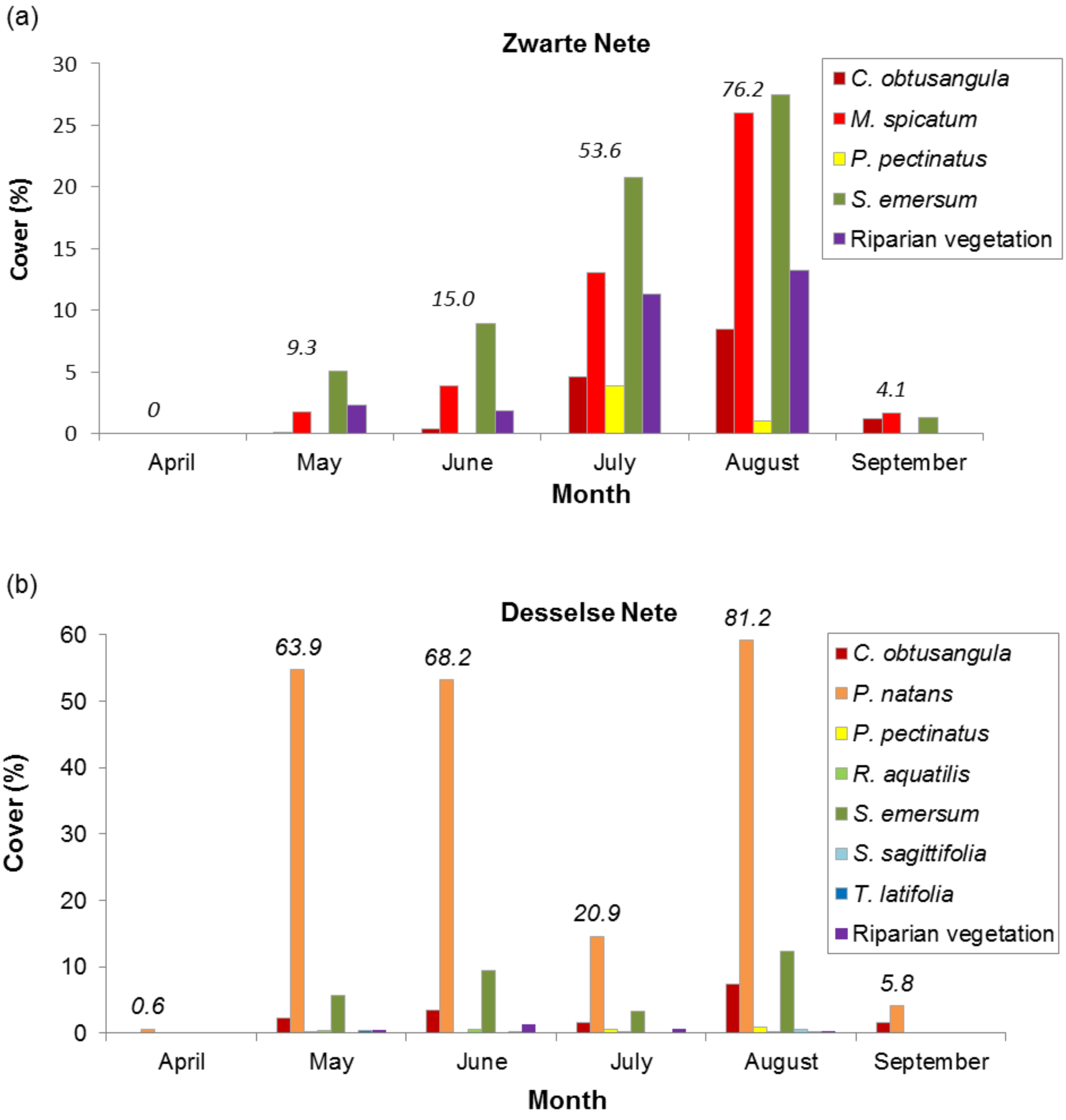

Figure 4: Vegetation cover per species per month for the reach in the **(a)** Zwarte Nete and **(b)** Desselse Nete. The colors of the bars refer to the species, the same colors for the species as in Fig. 3 are used (submerged species: red-yellow, floating species: green, emerged species: blue). The total vegetation cover per month is added in italics.

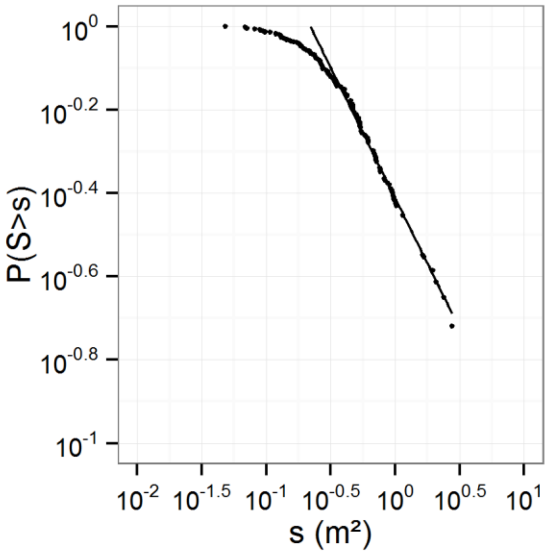

Figure 5: The inverse cumulative distribution of the patch sizes of *C. obtusangula* plotted on a double logarithmic scale. A power-law relationship is added with $\beta = 0.6$ of Eq.1 ($p<0.001$; $R^2 = 0.99$).

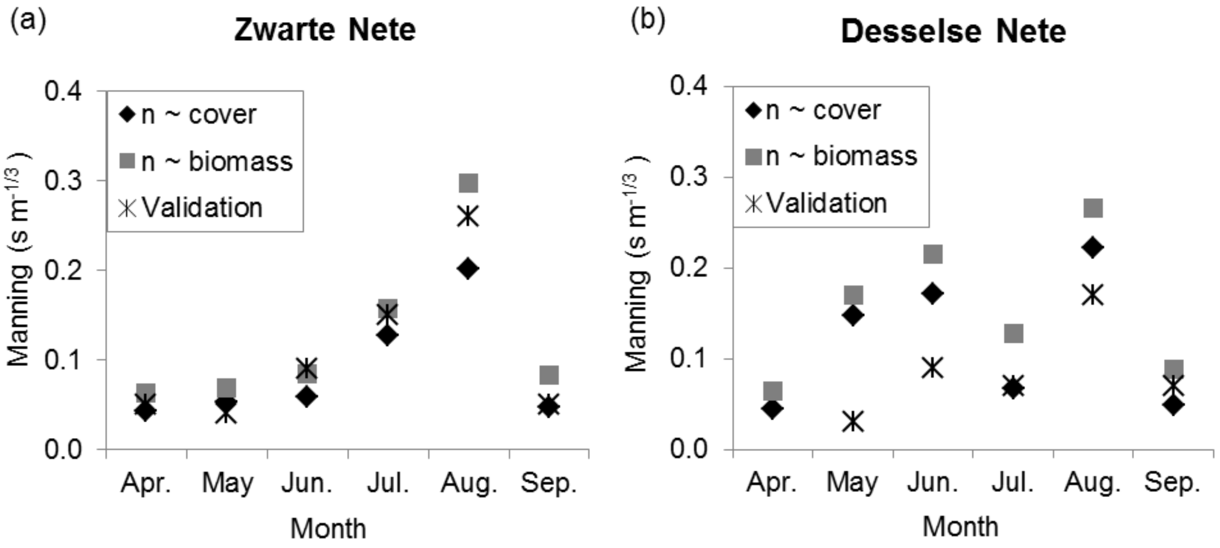

Figure 6: Manning coefficient in function of time for the **(a)** Zwarte Nete and **(b)** Desselse Nete. For the validation the Manning coefficient is calculated with Eq. 2(∗) based on field measurents, Table 1. The Manning coefficient is calculated with Eq. 3 (■) and Eq. 4 (♦), these are empirical relationships with cross-sectional blockage and biomass, respectively see Table 1.

Appendix

Table 6: Overview of the measured hydraulic data per river per month. These values are used to calculate the Manning coefficient with Eq. 2.

		April	**May**	**June**	**July**	**August**	**September**
Zwarte Nete							
Discharge	(m^3 s^{-1})	0.28	0.5	0.23	0.25	0.2	0.46
Cross-sectional area	(m^2)	1.06	1.39	1.28	1.97	2.36	1.69
Hydraulic radius	(m)	0.35	0.43	0.37	0.43	0.51	0.39
Water level slope	(m m^{-1})	0.0007	0.0007	0.0009	0.0012	0.0013	0.0005
Desselse Nete							
Discharge	(m^3 s^{-1})	0.45	0.61	0.33	0.39	0.32	0.61
Cross-sectional area	(m^2)	1.43	1.63	1.76	1.90	2.65	2.32
Hydraulic radius	(m)	0.38	0.33	0.44	0.46	0.57	0.52
Water level slope	(m m^{-1})	-	0.0005	0.0009	0.0006	0.0009	0.0008

Table 7: The biomass:cover conversion factor mean ± standard error (g m^{-2}) is measured per month for *C. obtusangula*, *S. emersum* and *P. natans* (n=3). Note that no replicates were taken in April, so no standard error is given.

	Apr.	**May**	**Jun.**	**Jul.**	**Aug.**	**Sept.**
C. obtusangula	28.5	NA	114.8 ± 37.7	123.7 ± 8.6	238.4 ± 50.3	354.9 ± 41.0
P. natans	146.0	116.6 ± 15.9	172.8 ± 45.3	209.8 ± 48.3	174.5 ± 19.5	190.6 ± 67.6
S. emersum	1.1	4.6 ± 1.7	49.9 ± 8.5	85.3 ± 14.0	202.2 ± 62.0	64.0 ± 10.7